Ultrasoft pseudopotentials applied to magnetic Fe, Co, and Ni: From atoms to solids

E. G. Moroni, G. Kresse, and J. Hafner
Institut für Theoretische Physik, Technische Universität Wien, Wiedner Hauptstrasse 8-10/136, A-1040 Wien, Austria

J. Furthmüller
Institut für Festkörpertheorie und Theoretische Optik, Friedrich-Schiller-Universität Jena, Max-Wien-Platz 1, D-07743 Jena, Germany
(Received 4 June 1997)

We present a study of the accuracy, transferability, and plane-wave convergence properties of ultrasoft Vanderbilt-type pseudopotentials for Fe, Co, and Ni in the context of atomic, molecular, and solid calculations. Special attention has been given to the magnetic properties of these systems. To go beyond the local-spin-density-approximation, generalized gradient approximations for the exchange-correlation functional have been included. All calculations have been performed using a plane-wave basis set, and we show that ultrasoft pseudopotentials allow – as expected – for a considerably lower cutoff energy than standard soft norm-conserving pseudopotentials. Lattice properties show very good agreement with all-electron calculations and experiment, while larger discrepancies exist for magnetic structural energy differences (which however remain smaller than 2 mRy/atom). These differences can be traced back to the frozen core approximation which is implicitly assumed in the construction of the pseudopotentials. More accurate results for the magnetization energies of atomic configurations can be obtained by treating the $3p$ semicore states as valence states. [S0163-1829(97)01347-7]

I. INTRODUCTION

During the past decade the development of *ab initio* molecular dynamics (MD) methods[1–3] within the density-functional local-density approximation has lead to a significant improvement in the understanding of material properties on an atomistic level and of temperature and time-dependent phenomena. However, applications to systems containing transition metals remain rare[4,5] and, in particular, no *ab initio* MD studies for extended magnetic systems have been published to date. Furthermore, for many systems (e.g., intermetallic compounds for permanent magnets or soft magnetic alloys) the complex interplay of the structural and magnetic degrees of freedom offers a challenging as well as promising field of application of *ab initio* MD techniques.

The reasons that have lead to this situations are, however, quite clear: with a few exceptions [e.g., the projector-augmented wave (PAW) method of Blöchl[6]] the most efficient *ab initio* MD methods work in a plane-wave basis and use pseudopotentials to describe the electron-ion interaction.[1,2,7,8] For *sp*-bonded metals and for the semiconducting elements the cutoff energy $E_{\rm cut}$ (i.e., the highest kinetic energy of a plane wave included in the basis set) is of the order of $E_{\rm cut} \leqslant 20$ Ry, corresponding to a basis of about 100 plane waves per atom. Although during the past decade many attempts have been made to optimize the plane-wave convergence of state-of-the-art normconserving pseudopotentials,[9–11] for transition metals the lower limit to the cutoff energy are of $E_{\rm cut} \geqslant 50$ Ry, resulting in basis sets of at least 400 plane waves per atoms.

The ultrasoft pseudopotential (USPP) first proposed by Vanderbilt[12] offers a possibility to resolve the problem of plane-wave convergence even for transition metals. Vanderbilt innovations consist of two fundamental steps: (a) the norm-conservation constraint is relaxed and the difference in the charge densities calculated from the all-electron and pseudo-orbitals is described in terms of a small number of localized augmentations functions. This allows us to construct extremely soft pseudo wavefunctions requiring only a very low cutoff energy, usually $E_{\rm cut}$ can be as low as 20–25 Ry.[8,12] (b) The freedom gained by relaxing the norm-conservation constraint is used to fit the scattering properties of the all-electron functions not only at one, but at two or more reference energies spanning the entire width of the valence band. This allows perfect control of the accuracy and transferability of the ultrasoft pseudopotentials.

USPP's have been implemented in *ab initio* MD codes by Laasonen *et al.*[13] and Kresse and Hafner[5] and applied successfully to the calculations of phonon-dispersion relations of crystalline transition metals,[14] to the study of the properties and reactions at transition metal surfaces,[15] and to the simulations of liquid transition metals.[4,5,16] However, to our knowledge no attempt has been made to use USPP's for the investigation of the magnetic properties of transition metals. Hence, one of the aims of the present work will be the assessment of the accuracy, transferability, and convergence properties of USPP for magnetic systems, ranging from the free atoms over clusters and monolayers to the crystalline metals. For magnetic systems, the problem of the transferability of a pseudopotential acquires even a new facet because a potential constructed for an atomic (and usually nonmagnetic) reference configuration will be used to perform calculations for nonmagnetic, ferromagnetic, and antiferromagnetic crystalline phases.

While the correct prediction of the magnetic moments is usually considered to be one of the major successes of local spin-density[17–19] (LSD) theory, one also has to remain aware of its limitations. In general, these limitations result in the well-known ''overbinding'' trend manifested in many LSD calculations: equilibrium lattice constant in solids are under-

estimated, cohesive energies and bulk moduli are overestimated compared to the experimental reference values. In systems showing strong magnetovolume effects (such as, e.g., Fe) this can lead to dramatic effects: for the solid phase of Fe the ground state is predicted to be nonmagnetic hexagonal-close-packed instead of ferromagnetic body-centered-cubic.

These well-known limitations of the LSD have motivated a continuous effort to improve the exchange-correlation (XC) functional within the framework of generalized gradient approximations[20] (GGA's) to density functional theory (DFT). The success of GGA's derives from their ability to correct many of the limitations of the LSD without increasing the computational cost significantly. Recently, Perdew and Wang[21] have presented a unified real-space-cutoff construction of a GGA for exchange and correlation (PW91), which shares several properties with the exact XC functional.[22] Many calculations on atoms, molecules, and solids have shown that the GGA improves the predictions of cohesive energy and other bulk properties. The ground state of Fe is a nice example where the GGA corrects a qualitatively wrong prediction of the LSD.[23,24] For materials and properties where the LSD is already a very good approximation the GGA tends to overcorrect the LSD error.[24]

The necessity to include nonlocal corrections to the exchange-correlation functional also reflects on the construction of the pseudopotentials. In this work, we use the same approximation for the exchange-correlation functional in the generation of the pseudopotential and in its various applications. Another difficulty arises from the fact that in pseudopotential calculations, the total charge density is subdivided into core and valence contributions. Since the exchange-correlation functional is nonlinear, this leads to inaccuracies in computing the valence core interactions that have to be corrected by applying nonlinear core corrections (NLCC's).[25] Besides, NLCC's are also of particular importance in magnetic applications[25–28] because the spin density (which is equal to the density of magnetic moments) is more localized around the atomic core than the charge density. Finally, the frozen core approximation for the $3p$ shell may be a problem in certain application for $3d$ metals, especially for those with a less than half filled d shell. Among the magnetic $3d$ metals, Fe is a boundary case: the broadening of the $3p$ levels into a band can become important under pressure. Hence, we also have to test corrections arising from treating the $3p$ ''semicore'' electrons as valence electrons.

The organization of the article is as follows. In Sec. II we briefly describe the computational method and the properties of the ultrasoft pseudopotentials. Results of transferability tests and computational details are also presented. Section III describes all-electron and pseudopotential calculations for atoms. We show that although the USPP results for the spin polarized atoms share the shortcomings of other LSD calculations (absence of multiplet structure, etc.), they are as accurate as all-electron LSD calculations. In Sec. IV we discuss the comparison of our USPP results for the properties of dimers with all-electron calculations. The magnetic effects for different multiplets are also outlined. In Sec. V we discuss the applications of USPP to hexagonal and squared monolayers of Fe, Co, and Ni, comparing with available full-potential linear augmented plane-wave (FLAPW) calculations. Results of computation of structural, electronic and magnetic properties for the solid metallic phases of Fe, Co, and Ni are given in Sec. VI, together with detailed comparison with the most accurate all-electron calculations. Final remarks are contained in Sec. VII.

II. METHOD

In this section we describe briefly the main features of the ultrasoft pseudopotentials and of the method of calculation.

A. Ultrasoft pseudopotentials

The ultrasoft Vanderbilt[12] pseudopotentials used in this work have been constructed in a very similar way as described by two of us in Ref. 8. The starting point is the construction of a very smooth non-normconserving pseudo wave function ϕ_ν^{US} for all required channels ν (defined for each set of quantum numbers nl, at one or two reference energies ϵ, i.e., $\nu=nl\epsilon$) satisfying the minimum requirement of being continuous and continuously differentiable at a large cutoff radius r_c^l. Following Rappe, Rabe, Kaxiras, and Joannopoulos[11] (RRKJ) we expand the pseudo wave functions inside the cutoff radii r_c^l in terms of a linear combination of spherical Bessel functions,

$$\phi_\nu^{\mathrm{US}}(r)=\sum_{i=1}^{n}\ \alpha_i\ r\ \mathrm{j}_l(q_i r),\qquad r<r_\mathrm{c}^l, \tag{1}$$

with the α_i and q_i chosen such that the logarithmic derivative of ϕ_ν^{US} agrees at r_c^l with the all-electron value. To satisfy this condition a minimal set of two spherical Bessel functions $\mathrm{j}_l(q_i r)$ is sufficient if no norm conservation is imposed. These wave functions are very smooth and only a low energy cutoff is required to describe them accurately with a plane-wave basis set. In practice, the Fe, Co, and Ni ultrasoft pseudopotentials have been generated for the nonmagnetic $4s^1 3d^7$, $4s^1 3d^8$, and $4s^1 3d^9$ atomic configurations, with cutoff radii $r_\mathrm{c}^l=2.2$, 2.45, 2.45 a.u. for the $4s$, $4p$, and $3d$ US wave functions, respectively. For each angular momentum l, two projectors were used with reference energies spanning a width of approximately 1–2 Ry.

Ultrasoft separable pseudopotentials can be constructed from these wave functions using Vanderbilt's scheme.[12,13,8] Differently to the the work of Vanderbilt[12] we ''pseudize'' the augmentation functions $Q_{\nu\mu}(\mathbf{r})$ by expressing them in terms of norm-conserving pseudo wave functions ϕ_ν^{NC} constructed with an augmentation radius r_{aug}^l much smaller than r_c^l,

$$Q_{\nu\mu}(\mathbf{r})=\phi_\nu^{\mathrm{NC}}(\mathbf{r})^*\phi_\mu^{\mathrm{NC}}(\mathbf{r})-\phi_\nu^{\mathrm{US}}(\mathbf{r})^*\phi_\mu^{\mathrm{US}}(\mathbf{r}). \tag{2}$$

To satisfy the requirements of normconservation and the continuity of the first two derivatives of the norm-conserving pseudo wave function at r_{aug}^l, a minimum of three spherical Bessel functions is needed in the expansion [see Eq. (1)]. For the normconserving wave functions the augmentation radii $r_{\mathrm{aug}}^l=2.2$, 2.2, and 1.9 a.u. were chosen.

The use of spherical Bessel functions to represent the wave functions allows a simple estimate of the required energy cutoffs. For the studied systems, an energy cutoff of $E_{\mathrm{cut}}=\hbar^2(1.35q_{\max})^2/(2m_e)$, where $q_{\max}$ is the maximum q_i

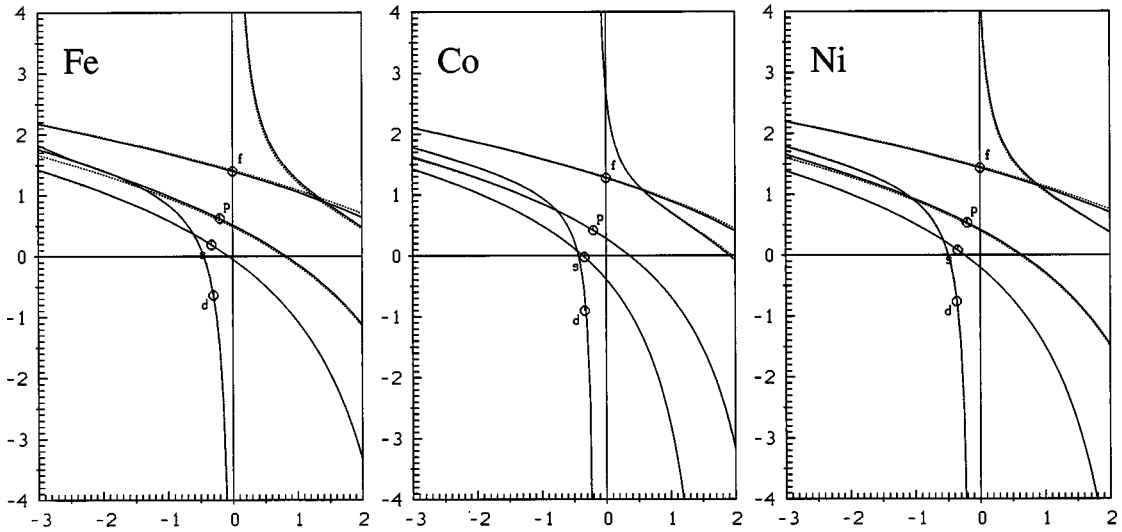

FIG. 1. Logarithmic derivatives at $r=2.2$ a.u. for the s, p, d, and f states of Fe, Co, and Ni atom. Solid lines: results of all-electron calculations. Dashed line: results using the ultrasoft pseudopotential without semicore states.

used in the expansion of the US wave functions guarantees an absolute energy convergence around 5 meV/electron, and $E_{\rm cut}=\hbar^2(1.15q_{\rm max})^2/(2m_e)$ an accuracy around 50 meV/electron. The quality of plane-wave calculations decays very rapidly if the cutoff is reduced below $E_{\rm min}=\hbar^2 q_{\rm max}^2/(2m_e)$. This convergence criterion predicts that a cutoff around 250 eV (18 Ry) is required to obtain an accuracy of 5 meV/electron. The plane-wave cutoff for a norm-conserving pseudopotential with the *same* quality would be around 700 eV (50 Ry) (but even in that case two d channels would be required to get a similar accuracy as for the US pseudopotential). Similar cutoffs for norm-conserving PP were reported by other authors.[29] This means that a calculation with a norm-conserving pseudopotential would need an approximately 4 times larger basis set, making calculations significantly more expensive than with the US pseudopotential. The average number of basis functions for the US pseudopotential is around 70–100 plane waves per atom, allowing simulations for up to 50–100 atoms on inexpensive workstations.

Considerable care has also been taken in the construction of the local PP $V_{\rm loc}$. The importance of higher angular components is often overlooked in the context of PP calculations, althought the inclusion of f states can change the volume considerably. A convenient choice for the local potential is usually a ''truncated'' AE potential. In this study, we replace the AE potential inside the cutoff radius $r_{\rm loc}=1.7$ a.u. by

$$V_{\rm loc}(r)=A\frac{\sin(q_{\rm loc}r)}{r} \quad \text{for} \quad r<r_{\rm loc}, \tag{3}$$

where $q_{\rm loc}$ and A are chosen so that the first derivative of the potential is continuous. If $r_{\rm loc}$ is chosen sufficiently small a very accurate description of the f states can be achieved. Another possible choice for the local potential is a pseudopotential constructed for the f states. But this potential is often so attractive, that ghost states in the s or p components cannot be avoided.[30]

To complement our study for Fe we have also generated an USPP in the $3p^6 4s^1 3d^7$ nonmagnetic configuration including the $3p$ semicore states as valence states. In this case the cutoff radii of the pseudo wave function were reduced to 1.9 a.u. and for a converged total energy the cutoff energy for the plane-wave expansions must be around 400 eV. This USPP gives a better transferability for high-pressure properties of the solid hcp phase of Fe (Ref. 31) and also for spin polarization properties in atoms and solids.

1. Transferability and convergence tests

Figure 1 shows the logarithmic derivatives at $r=2.2$ a.u. for the AE and US wave functions for each l in the case of Fe, Co, and Ni. As can be seen from Fig. 1 the scattering properties of the pseudo wave function are very accurate not only for the $l=0-2$ components but also for the unbound $l=3$ (f states) over a wide range of energies.

Convergence tests for total energy and magnetic properties of Fe, Co, and Ni in atoms, dimers, monolayers, and in the solid have been performed using the LSD and the GGA functionals. Here we have chosen to show tests for the solid only. Figure 2 displays the convergence of the cohesive energy and of the magnetic moment against $E_{\rm cut}$ for the ferromagnetic (FM) and nonmagnetic (NM) phases of bcc Fe and fcc Ni using the GGA XC functional. To compare the cohesive energies with experiment one should also add the atomic spin polarization energy. It can be seen, that the cohesive energies and magnetic moments for both NM and FM phases converge around 250 eV. At this cutoff structural energy differences are converged within 1 meV and the error in the magnetic moment is smaller than $0.01\mu_B$. By increasing $E_{\rm cut}$ to 300 eV the absolute error in the total energy becomes smaller than 1 meV/atom.

2. Nonlinear core corrections

To describe the valence core energy interaction accurately the nonlinear core correction (NLCC) scheme proposed by Louie, Froyen, and Cohen[25] has been used. The main idea of this approach is to compute the XC energy $E_{\rm xc}$ seen by the valence electrons using the total rather than the valence charge density $n_v(r)$. The inclusion of the core charge $n_c(r)$

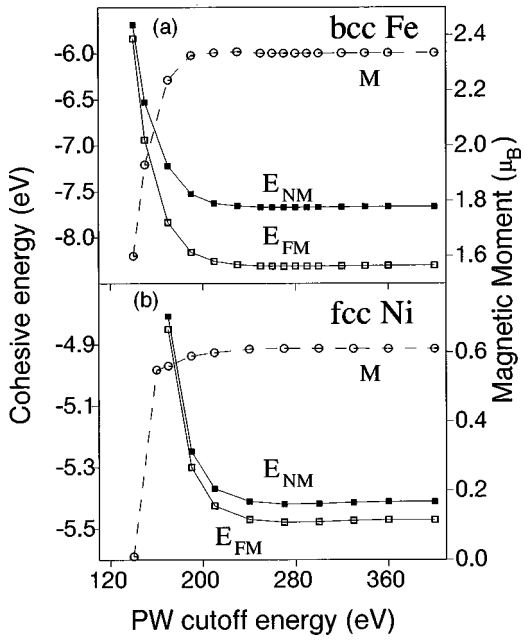

FIG. 2. (a) Cohesive energies (with respect to the nonmagnetic atom) and magnetic local moment versus plane-wave cutoff energy for the nonmagnetic (NM) and ferromagnetic (FM) solid phases of bcc Fe in the ultrasoft pseudopotential approach. (b) Same as in (a) but for fcc Ni.

gives a more accurate representation of the nonlinear dependence of E_{xc} and v_{xc} in systems where core and valence charge overlap. It is of crucial importance for an accurate description of magnetization energies as indicated by previous calculations,[25–28] because in $3d$ transition metal atoms the $3d$ valence states overlap significantly with the $3p$ semicore states; thus the spin polarization function $\zeta=[(n_\uparrow-n_\downarrow)]/n$ is much smaller than the respective valence spin polarization ζ_v.

As all other quantities, the core charge density has to be pseudized within the core region. Because GGA requires that the second derivative is continuous we expanded the core charge density inside a cutoff radius r_{pc} in a set of two Bessel functions j_0,

$$\sum_{i=1,2} B_i \frac{\sin(q_i r)}{r}, \tag{4}$$

where q_i and B_i are chosen so that the first two derivatives of the partial core charge density are continuous (the scheme works basically along the same lines as the construction of the ultrasoft wave functions for $l=0$).

Tests on the FM and NM solid phases indicate that a cutoff of $r_{pc}=1.2$ a.u. is sufficient within our scheme to get highly converged values for the equilibrium volume, bulk modulus, and structural energy. When we decreased the cutoff r_{pc} from 1.2 a.u. to 0.6 a.u. the equilibrium volumes changed by less than 0.1%, and structural energy differences by less than 1 meV. The quantities which are most sensitive to the NLCC are the total moment, the exchange splitting and the magnetic energy (i.e., the energy difference between the FM and NM phase). The influences of NLCC's for these quantities is shown in Table I. It is found that the local moment, the exchange splitting of the uppermost $3d$ bands, and the respective magnetic energy are largely overestimated if one chooses a too large cutoff radius r_{pc}, confirming the importance of NLCC for describing magnetic effects. Nevertheless with $r_{pc}=1.2$, all values are practically converged.

TABLE I. Effects of partial core correction on the transferability of LSD USPP of Fe and Co for the magnetic properties of ferromagnetic bcc Fe and hcp Co. All calculations have been done at the experimental volume of the ground state. r_{pc} is the cutoff radius for the partial core corrections, ξ denotes the exchange splitting for the uppermost $3d$ band, and E_m is the magnetic energy (energy difference between FM and NM phase) computed at the experimental lattice constant.

	r_{pc} (a.u.)	M μ_B	ξ (eV)	E_m (eV)
	1.6	2.52	3.24	0.71
bcc Fe	1.2	2.23	2.52	0.48
	0.6	2.23	2.52	0.48
	1.6	1.66	2.10	0.33
hcp Co	1.2	1.58	1.73	0.20
	0.6	1.57	1.70	0.19

B. Computational method

Most calculations presented here have been done with a spin polarized version of the Vienna *ab initio* simulation package (VASP).[3] A detailed description of VASP and its algorithms can be found in Ref. 3. VASP is a first-principle plane-wave code based density-functional theory and allows the use of USPP. The solution of the generalized Kohn-Sham equations is performed using an efficient iterative matrix diagonalization routine based on a sequential band-by-band residuum minimization method – direct inversion in the iterative subspace (RMM-DIIS).[3,32] Alternatively, a matrix diagonalization based on a preconditioned band-by-band conjugate gradient (CG) algorithm[2,3,7] can be used. The charge density is updated using an improved Pulay mixing.[3,33] The efficiencies of different iterative schemes for the calculations of the ground state in paramagnetic Fe as a function of the size of the cell are compared in Ref. 3.

For the exchange-correlation energy we have considered the LSD and the GGA approximations. For LSD, we used the exchange-correlation results of Ceperley and Alder[34] as parametrized by Perdew and Zunger[35] (CA-PZ) while for the GGA functional we have used the (PW91) (Ref. 21) form. The approach of White and Bird[36] has been used to compute the GGA spin-polarized-exchange-correlation potentials. For intermediate spin polarizations the interpolation formula of von Barth and Hedin[37] is applied. For specific cases, however, we have also tested the spin interpolation for the correlation energy proposed by Vosko-Wilk-Nusair (VWN),[38] which leads to slightly different results substantiating the importance of the spin dependence of the correlation energy and of the interpolation procedures.[38,39]

Brillouin zone integrations in our calculations was performed on a grid of Monkhorst-Pack special points[40] using different schemes. The linear tetrahedron (LT) method including the corrections according to Blöchl *et al.*[41] has been

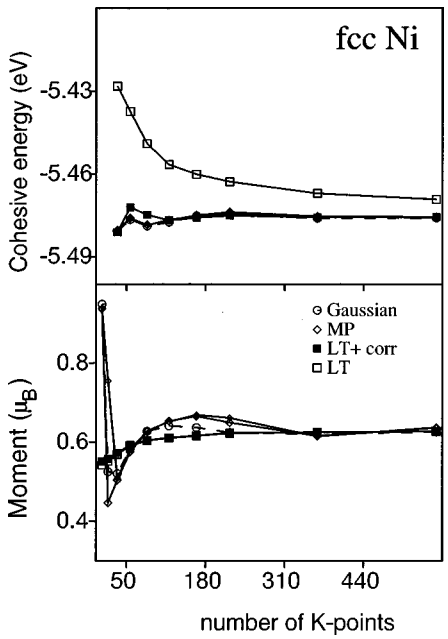

FIG. 3. Comparison between different integration methods using an USPP and the GGA approximation for fcc Ni. Convergence properties of total energy, magnetic energy, and magnetic moment for fcc Ni at $a_0=6.52$ Å versus number of k points. (a) Linear tetrahedron (open square) (b) Linear tetrahedron with Blöchl correction (filled square) (c) Methfessel-Paxton method (open diamond), (d) Gaussian smearing (open circle). For all smearing methods δ equals 0.2 eV.

chosen for the solid phases. This method is rapidly convergent with respect to the k-point grid. Approximately 100 k points in the irreducible wedge of the Brillouin zone are required to converge the structural energy differences even for FM phases within 1 meV. As an example, we show in Fig. 3 the convergence of the magnetic moment and the cohesive energy of fcc Ni versus the number of k points for different Brillouin zone integrations methods. Using the LT method the convergence is rather slow, compared to the finite temperature smearing methods and to the tetrahedron method with the corrections of Blöchl *et al.*[41] Smearing methods based on finite temperature DFT (Ref. 42) with a Gaussian or Methfessel and Paxton[43] broadening function give a similar convergence as Blöchl's method with the advantage that the calculation of forces is efficient and convenient (in Blöchl's method forces are difficult to calculate accurately).[3]

III. ATOMS

Tests of transferability of ultrasoft pseudopotentials are described hereafter for Fe, Co, and Ni atoms. The results of USPP calculations for magnetic properties are compared with the respective all electron results.

A. All-electron results

Fe, Co, and Ni atoms are spin polarized and have 8, 9, and 10 valence electrons, respectively, distributed over the $3d$ and $4s$ levels (five electrons in the $3d$ spin-up levels, two occupying the $4s$ levels, and the rest in the $3d$ spin-down levels). Hund's first rule of maximum multiplicity is insofar obeyed, that the atoms have magnetic moments of $4\mu_B$, $3\mu_B$, and $2\mu_B$.

TABLE II. Comparison of LSD and GGA USPP and scalar relativistic all-electron calculations for Fe, Co, and Ni atoms. For each atom we list the computed ground state (gs) configuration. Magnetic energy $\Delta E_m=E_{\text{ground}}-E_{\text{NM}}(4s^1 3d^{n-1})$ (see text) and interconfigurational energy ΔE_{ic} (see text) are in eV. The GGA results are in parentheses.

		USPP		AE	EXP
Fe	gs	$3d^{6.2}4s^{1.8}$	$3p^6 3d^{6.2}4s^{1.8}$	$3d^{6.2}4s^{1.8}$	$3d^6 4s^2$
	ΔE_m	2.82 (3.15)	(2.99)	2.60 (2.76)	
	ΔE_{ic}	0.45 (0.59)	(0.54)	0.37 (0.39)	0.87
Co	gs	$3d^{7.7}4s^{1.3}$		$3d^{7.7}4s^{1.3}$	$3d^7 4s^2$
	ΔE_m	1.28 (1.43)		1.22 (1.31)	
	ΔE_{ic}	-0.40 (-0.31)		-0.41 (-0.42)	0.42
Ni	gs	$3d^9 4s^1$		$3d^9 4s^1$	$3d^8 4s^2$
	ΔE_m	0.49 (0.55)		0.45 (0.52)	
	ΔE_{ic}	-1.18 (-1.14)		-1.20 (-1.21)	-0.03

The experimental ground state configurations are shown in Table II in the column EXP. One major problem of LSD and GGA calculations is that they predict the wrong ground state. Results for the AE ground states if partial occupancies are allowed and spherical symmetry is assumed are shown in Table II. We have obtained these ground states by simply varying the occupancies in a spherical AE program by hand and determining the lowest energy configuration. The reason for this wrong ground state can be traced back to the wrong description of the interconfiguration energy $\Delta E_{\text{ic}}=E(4s^1 3d^{n-1})-E(4s^2 3d^{n-2})$, and has been reported in literature before. Harris and Jones[44] have, for instance, shown that LSD favors d occupancies and pushes down the $3d^{n-1}4s^1$ configuration by nearly 1 eV with respect to the $3d^{n-2}4s^2$ configuration. We obtain similar results for AE LDA and GGA calculations (Table II).

Baroni[45] has shown that for the Fe series a careful treatment of the self-interactions including non spherical contributions dramatically improves the LSD results for ΔE_{ic}. A similar improvement over LSD and GGA is obtained in configuration interaction procedures[46] or quantum Monte Carlo calculations.[52] The objective of the current paper is anyway a comparison between pseudopotential and AE calculations, thus we will not comment further on these problems.

B. Pseudopotential results

For computing the energy of atoms with the USPP's we have used a large cubic unit cell with $a_0=10$ Å and sampled the wave functions at the Γ point only. Magnetic energies ΔE_m are evaluated directly by subtracting from the total energy of the spin-polarized free atom in the cubic box the energy of the nonmagnetic pseudoatom in the reference configuration $4s^1 3d^{n-1}$. To calculate the interconfigurational energy, the occupancies of the $4s$ and $3d$ levels for both spins have been fixed by hand and the electronic minimiza-

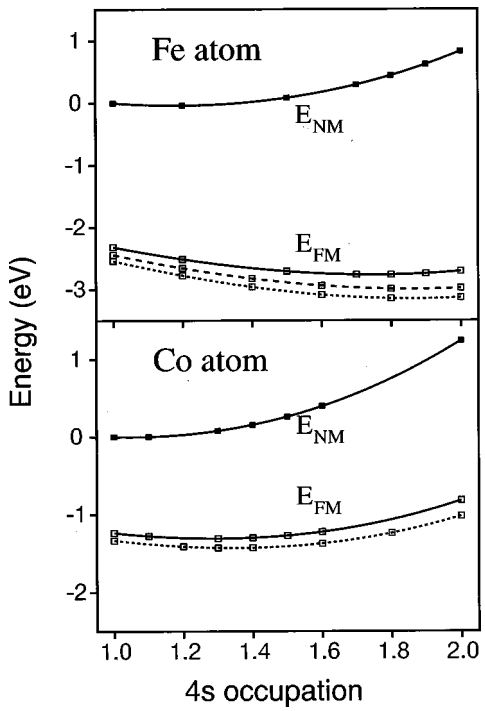

FIG. 4. Magnetic and nonmagnetic GGA atomic energy of Fe and Co atoms versus $4s$ valence electrons composition, using the (a) all-electron method [(solid lines)], (b) ultrasoft pseudopotential without semicore states (small dashed lines), (c) ultrasoft pseudopotential with $3p$ semicore states (long dashed line).

tion was performed in a way that preserves the ordering of the $4s$ and $3d$ eigenvalues. In all cases spherical symmetry was conserved to allow direct comparison with the AE calculations.

In Table II the USPP calculations for the ground state properties of spin-polarized Fe, Co, and Ni atoms are summarized and compared with all-electron results for the LSD and GGA functionals. The USPP calculations give exactly the same ground state as the AE calculations. The errors for the spin-polarization energy ΔE_m and the interconfigurational energy are also quite small (in the 5–10 % range). Most of these errors are probably due to the frozen core approximation. Evidently the transferability of Fe USPP is improved when $3p$ electrons are treated as valence states. In this case, ΔE_m reduces from 3.15 eV to 2.99 eV using GGA (see Table II) to be compared with the all-electron value of 2.76 eV.

In Fig. 4 we show the USPP GGA atomic energies for the NM and FM configurations of Fe and Co atoms compared with the respective AE GGA atomic energies at different $4s$-state occupancies. The zero energy reference coincides with the nonmagnetic $4s^1 3d^{n-1}$ atomic configuration. The nonmagnetic energies for the PP and AE calculation differ by at most 20 meV and the two curves are therefore not distinguishable in Fig. 4. In Fe and Co atoms contrary to Ni atom, the magnetic energy increases by filling the $4s$ orbitals.

All these findings demonstrate good transferability of LSD and GGA USPP in the context of atomic calculations. However, one should keep in mind that GGA corrections are not sufficient for reproducing the experimental atomic ground state.

IV. DIMERS

In this section we extend the test of USPP to the FM and NM configurations of Fe, Co, and Ni dimers. The formation of the dimer is accompanied by a decrease of total energy and by a lowering of the spin moment compared to the spin-polarized free atoms. The dimers have a nearly continuous spectrum of energy levels and it costs little energy to transfer electrons from weakly bonding to weakly antibonding orbitals. This reflects the competition between Hund's multiplicity rule (which tends to maximize the spin multiplicity) and energy minimization (which usually leads to low-spin configurations). The dense eigenvalue spectrum makes convergence to the electronic ground state in general difficult.

The potential energy curves $V(r)$ of the FM and NM configurations for each molecule have been computed using the LSD and GGA approximations. We have used a simple cubic unit cell with $a_0=10$ Å and sampled the wave functions at the Γ point only. To improve energy stability we had to introduce partial occupancies using Gaussian broadening with a width of $\sigma=0.2$ eV (all energies were extrapolated to zero temperature according to Refs. 42 and 3). The electronic minimization is accelerated by starting from a superpos,ition of spin-polarized atomic charge densities. The potential energy curves $V(r)$ have been fitted with the modified Morse potential of Hulburt and Hirschfelder[47]

$$V(r)=D_e[(1-e^{-\beta x})^2+b\beta^3 x^3 e^{-2\beta x}(1+a\beta x)-1], \tag{5}$$

where $x=r-r_e$ and r_e and D_e are the equilibrium distance and bonding energy, respectively.

In Table III, the computed equilibrium distance r_e, the binding energy D_e, and the vibrational frequencies ω_e of the dimers are shown and compared to the available experimental data and all-electron calculations. Extensive comparisons are possible for the Fe_2 dimer since its magnetic and equilibrium configurations have been a subject of intense investigations in recent years. Rare gas matrix isolation techniques[48] in combination with x-ray absorption fine structure (EXAFS) and high temperature mass spectroscopy have been used to estimate the bond lengths (r_e) and the dissociation energy (D_e) of transition metal dimer. The measured r_e of Fe_2 in argon and the less polarizable neon matrices are 1.85 and 2.02 Å, respectively, while the most recent estimates of D_e are between 1.14 eV and 1.6 eV.[48] Theoretical calculations have led to conflicting conclusions: Most of the calculations based on the Hartree-Fock (HF) methods support a low-spin state. On the other hand LSD (Ref. 49) and GGA (Ref. 50) calculations predict the $^7\Delta_u$ as the ground state. This result has been confirmed recently by a CI calculation,[51] which gave $r_e=2.06$ Å and $D_e=1.57$ eV.

For the Fe_2 dimer we find $r_e=2.00$ Å (2.03 Å) using the USPP without (with) semicore $3p$ states using the GGA approximation. The results for r_e agree very well with the calculations of Castro and Salahub[50] and the CI results of Mitas.[52] The vibrational frequency ω_e is very sensitive to the XC potentials and to the exact method of calculation, and

TABLE III. Calculated equilibrium bond-length (r_e), vibrational frequency (ω_e), and dissociation energy (D_e) for Fe_2, Co_2, and Ni_2 dimers in their FM ground state and for the NM excited state. USPP results for LSD and GGA are compared with previous calculations and experiment. GGA results are in parenthesis. For each calculation we also indicate the used exchange-correlation type. For the Fe atom the USPP ps1 was generated for the $4s^1 3d^7$ and ps2 for the $3p^6 4s^1 3d^7$ atomic configurations (i.e., treating the $3p$ electrons as valence electrons). For the USPP calculations D_e is evaluated with respect to the spin-polarized atoms.

Dimer	State	Method	xc type		r_e (Å)		ω_e (cm^-1)		D_e (eV)	
			LSD	(GGA)						
	FM	LCAO [a]	VWN	(PW86)	1.96	(2.00)	497	(474)	4.38	(3.24)
	FM	LCAO [b]	RSK-vBH		1.96		412		4.05	
	FM	LMTO [f]	GL		2.09		390		3.45	
Fe_2	FM	PAW [c]	CA-PZ		1.94		441		3.99	
	FM	This work (ps1)	CA-PZ	(PW91)	1.91	(2.00)	400	(363)	3.94	(3.13)
	FM	This work (ps2)		(PW91)		(2.03)		(350)		(3.21)
	FM	CI [d]			2.06		485		1.57	
	FM	Exp [e]			1.85, 2.02		300		1.14, 1.06	
	NM	LCAO [a]	VWN	(PW86)	1.80	(1.83)			2.06	(0.69)
	NM	LCAO [b]	RSK-vBH		1.83		461		1.73	
	NM	This work (ps1)	CA-PZ	(PW91)	1.74	(1.79)	535	(497)	1.94	(0.41)
	NM	This work (ps2)		(PW91)		(1.81)		(493)		(0.73)
	FM	LMTO [f]	GL		2.07		360		3.35	
Co_2	FM	This work	CA-PZ	(PW91)	1.91	(1.97)	407	(385)	4.58	(3.88)
	NM	This work	CA-PZ	(PW91)	1.90	(1.96)	410	(369)	2.95	(2.02)
	FM	LMTO [f]	GL		2.18		320		2.70	
Ni_2	FM	This work	CA-PZ	(PW91)	2.04	(2.11)	342	(318)	3.59	(3.06)
	FM	Exp [g]			2.12				2.20	
	NM	This work	CA-PZ	(PW91)	2.04	(2.11)	339	(318)	3.19	(2.61)

[a]Reference 50.
[b]Reference 49.
[c]Reference 6.
[d]Reference 52.
[e]Reference 48.
[f]Reference 44.
[g]Reference 75,

large discrepancies (~ 100 cm^{-1}) are found between different AE LSD calculations. The estimated error (fitting accuracy, broadening technique, and finite size effects) in w_e in our calculation is of about 50 cm^{-1}.

Our calculated binding energies D_e compare well with all-electron results. GGA corrections decrease the binding energy by about $\sim$ 0.8 eV for the USPP and $\sim$ 1.0 eV for the LCAO methods. However, the binding energy D_e for Fe $_2$ is still a factor of two too large compared to the experimental and the CI value. The energy difference between the FM and NM configurations in Fe_2 is 2.0 eV and 2.7 eV using LSD and GGA. These values can be compared with the results of the LCAO method which are 2.32 eV and 2.55 eV.[50] If we compute the GGA spin energy using the USPP including $3p$ states we find $\Delta E = 2.5$ eV which compares very well with the AE result. The ferromagnetic interaction leads to an increase of 0.2 Å (or 10%) for the equilibrium bond length, while in Co_2 and Ni_2 this difference is practically zero, indicating a smaller coupling between magnetism and bond length.

For Co_2 and Ni_2 dimers our r_e, ω_e, and D_e do not compare very well with the linear muffin-tin orbital results of Harris and Jones.[44] The main differences are probably due to insufficient accuracy of the muffin-tin approximation in molecular total energy calculations and due to the fact that the magnetic energies have been estimated perturbatively in Ref. 44.

In conclusion, we have demonstrated the possibility to use an USPP for studying spin and spectroscopic properties in $3d$ dimers. A systematic comparison with available all-electron and experimental results has been presented for the FM and NM configuration of Fe_2. For transition metal dimers the USPP approach is as accurate as the best available all-electron method, and is able to reproduce the magnetic energy of the high-spin ground state as a function of bond length. We expect a similar accuracy also for other transition metal dimers.

V. MONOLAYERS

Ultrathin films approaching a single monolayer are the prototype systems for investigating magnetism in reduced dimension. A comprehensive account of first-principle calculations of magnetic properties of thin films and related refer-

TABLE IV. Structural and magnetic properties for FM Fe, Co, and Ni monolayers with square and hexagonal structure computed using USPP and the LSD and GGA functionals. GGA results are given in parenthesis. For each system, a_{FM} is the interatomic distance and $\Delta a/a$ measures the magnetic strain with respect to the NM equilibrium. M is the local-spin moment while $\Gamma_m = \partial \ln M/\partial \ln a$ is the respective magnetic Grüneisen coefficient. E_m measures the energy difference between the NM and FM phases at their equilibrium positions and $E_{\mathrm{squ}}-E_{\mathrm{hex}}$ are the respective structural energy differences.

Structure		a_{FM} (Å)	$\Delta a/a$ (%)	M (μ_B/atom)	Γ_m	E_m (mRy/atom)	$E_{\mathrm{squ}}-E_{\mathrm{hex}}$ (mRy/atom)
	Fe	2.13 (2.33)	2.8 (7.7)	1.2 (2.7)	15.2 (1.7)	2.9 (24.5)	
Square	Co	2.18 (2.25)	2.7 (3.1)	1.7 (1.9)	1.4 (1.2)	18.0 (30.9)	
	Ni	2.20 (2.27)	0.9 (0.8)	0.8 (0.9)	1.9 (1.6)	5.1 (7.7)	
	Fe	2.32 (2.42)	3.8 (5.3)	2.3 (2.6)	3.1 (2.1)	26.2 (43.8)	24.1 (24.9)
Hexagonal	Co	2.28 (2.36)	1.7 (2.5)	1.7 (1.8)	2.0 (1.3)	24.3 (34.3)	23.7 (19.8)
	Ni	2.29 (2.36)	0.4 (0.4)	0.7 (0.8)	2.7 (1.3)	1.1 (5.5)	25.8 (24.0)

ences can be found in a recent review article.[53] Here the main focus is to test the USPP for their ability to describe the change of the magnetic structure as a function of structure and nearest neighbor distance for NM, FM, and AF squared and hexagonal Fe, Co, and Ni unsupported monolayers.

Calculations were performed with LSD and GGA; for Co and Ni we use a cutoff of 250 eV, while for Fe we use the USPP including $3p$ states with a cutoff of 400 eV. For the square and hexagonal lattice we have considered the $p(1\times1)$ NM and FM structure and the c(2×2) AF structure. The calculations are performed using eight layers of vacuum and the k-space integration is done with a $(11\times11\times3)$ Monkhorst Pack[40] grid (42 points in the irreducible wedge) using the smearing methods based on generalized finite temperature DFT with the Methfessel and Paxton broadening functions.[43,3] With the above parameters the total energy convergence is in the meV range and for the spin moments the error is below $0.01\mu_B$. The convergence with respect to the k points has been tested for the hexagonal FM Fe monolayer [with atom position constrained to the Cu(111) surface] using 5, 24, 42, and 99 k points; the corresponding cohesive energies are $E_c=-6.621$, -6.673, -6.682, -6.680 eV/atom while the computed moments are $M=2.91$, 2.86, 2.90, and $2.90\mu_B$, demonstrating the fast convergence of the k-point integration scheme. We have also performed tests with respect to the vacuum width and found that errors are below 1 meV/atom with eight layers of vacuum.

The computed structural and magnetic properties of Fe, Co, and Ni unsupported FM monolayers are listed in Table IV. The USPP LSD results for the equilibrium interatomic distance a_{FM}, the spin moment M, the magnetic energies and the structural energy difference $\Delta E_s=E_{\mathrm{squ}}-E_{\mathrm{hex}}$ for the FM, AF, and NM phases are compared with the LSD FLAPW results obtained by Pentcheva and Blügel in Ref. 54. For the Fe, Co, and Ni monolayer, both methods give practically equal plots of total energy and magnetic properties versus interatomic distances and very similar values for the equilibrium distances (within 1%), spin moment (within 5%) and magnetic energy (E_m) and structural energies differences ΔE_s (below 10 meV/atom). Both methods predict also the same ground state. The differences between the two methods are very small and are probably due to the different BZ samplings and different local-density exchange-correlation parametrization.

In Fig. 5 we show the dependence of the total energy of the NM, AF, and FM square and hexagonal Fe monolayers on the lattice constant. Both LSD and GGA functional have been used. The FM monolayer with hexagonal structure is the ground state. FM ordering in Fe is more stable than the AF and NM configurations. The square monolayer becomes stable at small nearest neighbor distances (for $a<2.1$ Å). However, the magnetic structure for Fe is not easy to establish by first-principle methods because of the sensitivity with respect to the exchange-correlation potential; for the square geometry GGA stabilizes the FM order with $M=2.7\mu_B$ while LSD favors NM and AF configurations. Table IV also summarizes the GGA results for Co and Ni monolayers. The $p(1\times1)$ hexagonal structure has the lowest energy and a stable FM moment for all Fe, Co, and Ni monolayers. The total energy differences ΔE_s between the square and hexagonal FM monolayer are nearly unaffected by the GGA corrections, while for all spin-dependent properties the spread between LSD and GGA results is significant. For the Fe, Co, and Ni hexagonal monolayers, GGA increases the LSD local moment M by 0.3, 0.1, and $0.1\mu_B$, respectively, and enhances considerably the exchange-correlation part of the

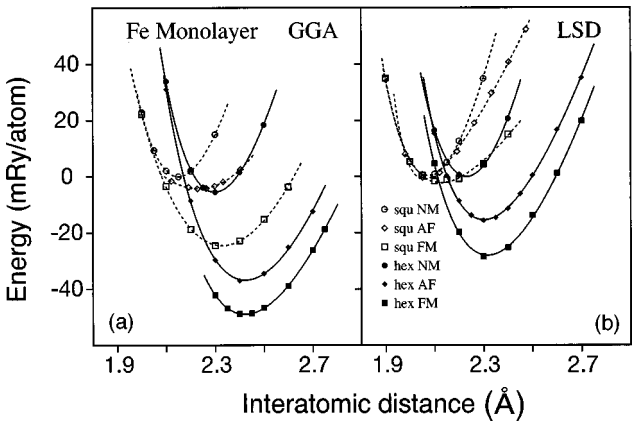

FIG. 5. Total energy as a function of interatomic distances of nonmagnetic (NM), ferromagnetic (FM) and antiferromagnetic (AF) square (SQU), and hexagonal (HEX) unsupported Fe monolayer. (a) GGA and (b) LSD USPP calculations.

magnetic energies. The reduction of the magnetic Grüneisen coefficient Γ_m and the enhanced magnetolattice effect $\Delta a/a$ are a measure of the increased FM stability (see Table IV) when using the GGA functional.

In conclusion it has been shown that an USPP may be used also for studying magnetic properties in thin metallic layer with an accuracy comparable to the best all-electron methods. GGA's leads to significant changes in the magnetic properties of Fe, Co, and Ni monolayers but predict the same ground state as LSD calculations. The structural energy difference between AF square and FM hexagonal reconstruction (of importance in Mn and Cr but not in Fe) depends strongly on the GGA corrections.[55]

VI. SOLID PHASES

In this section we check the accuracy of USPP calculations for describing the equilibrium and nonequilibrium solid phases of Fe, Co, and Ni. The quality of USPP using both the LSD and GGA functional is analyzed for the structural and magnetic properties, dealing also with properties of metastable phases which are not so directly subject to experimental study.

A. Ground state and band structure properties

The ground state properties for the experimentally stable crystal structures are obtained from Murnaghan[56] fits of the total energies computed at different volumes. In Table V we summarize our results for the lattice constant a_0, the bulk modulus B_0, the magnetic spin moment M_0, and the cohesive energy $E_{\rm coh}$ for the ground state of Fe, Co, and Ni. The cohesive energies $E_{\rm coh}$ are computed by subtracting from the total energies of the solids in their ground state the respective total energies of the pseudoatoms in their ground state spin configuration.

1. Comparison of USPP and AE results

With GGA the experimental ground state structure is the energetically most favorable one for all studied systems: bcc FM for Fe, hcp FM for Co, and fcc FM for Ni. GGA also increases the lattice constants considerably giving a better agreement with experiment. >From Table V it is clear that both LSD and GGA USPP results for a_0 are in excellent agreement with the respective full-potential results, while differences of about 5–10 % are found between USPP and AE calculations for B_0. Calculations of B_0 are more sensitive than a_0 to k-points sampling, cutoff energy convergence, and to the inclusion of semicore states in the USPP. For the USPP including $3p$ states, B_0 for FM bcc Fe is, for instance, 1.66 Mbar, whereas without semicore states the bulk modulus is only 1.50 Mbar. Finally, the differences between AE and USPP cohesive energies listed in Table V are mainly due to the differences in the choice of the reference atomic configuration.

The all-electron results for the spin moments, by far dominated by their d-electron part, are fairly well reproduced using USPP, the errors are 3% for Fe and 1% for Co and Ni. The computed spin moment pressure derivatives $\partial \ln M_s/\partial P$ are given in Table VI and compare well with the results of Moruzzi, Janak, and Williams[57] of $\partial \ln M_s/\partial P = -0.49$, -0.17 and -0.21 mbar^{-1} for bcc Fe, fcc Co and Ni, respectively. Comparison with experimental values[58] as shown in Table VI is also satisfactory, even though the pressure dependence of orbital moments is not included in this work. We want to point out that the choice for the spin interpolation of the LSD correlation energy may change the spin moment slightly. With the PZ-CA parametrization the spin moment is $2.05\mu_B$ for bcc Fe ($1.52\mu_B$ for hcp Co), whereas the VWN increases the spin moment to $2.11\mu_B$ ($1.53\mu_B$).

For all studied magnetic metals we note a good agreement between the USPP and all-electron spin-polarized density of states and band structures.[59,60,57,55] As seen from Fig. 6 the spin-polarized USPP bands cannot be modeled by rigidly shifting the paramagnetic band structure with an appropriate exchange splitting ξ. On a coarse scale both majority and minority DOS functions look similar, but looking in details there are larger differences in Fe, while in Ni the differences are relatively small. A comparison of selected exchange splitting and eigenvalues obtained using USPP and FLAPW methods is given in Table VII for the LSD and GGA functional. The width of the $3d$ bands in Fe including unoccupied states is estimated by the difference $E(N_3)$-$E(N_1)$.[61] We find a width of 5.2 eV for the majority spin and a width of 6.1 eV for the minority spin in agreement with all-electron results.[59,62,61] Moreover, the computed LSD (GGA) ratio of $N^{\uparrow}(\epsilon_F)/N^{\downarrow}(\epsilon_F) = 3.28$ (3.40) is consistent with the full-potential values of 3.14 (3.27) (Ref. 59) and this good agreement is also maintained for the total DOS which at ϵ_F is 1.07 (1.10) states/eV/atom.

2. LSD versus GGA using ultrasoft pseudopotential

Figure 7 summarizes the comparison between the LSD and GGA functional using USPP's for the phase stability, equilibrium volumes, and bulk moduli of the solid phases of Fe, Co, and Ni. In agreement with previous work[23,24] it is found that GGA increases the calculated equilibrium volumes, and reduces the bulk moduli, improving the agreement with experiment for $3d$ elements and correctly predicts for Fe the FM bcc structure as the ground state.

Large volume FM phases are favored by GGA more than low volume AF or NM phases. This is because spin-density inhomogeneities become rather important when volumes are large (as in bcc Fe and Co), leading to larger gradient corrections. GGA therefore leads to a nonuniform increase of the magnetic energy as shown in Fig. 8. It leads also to a general lattice expansion (correlated with the respective magnetic state) and to a smaller bulk modulus for all studied systems. In the case of Fe, the stabilization of the bcc phase arises almost entirely from the enhancement of the magnetic energy while the total energy difference between paramagnetic fcc-bcc crystal structure ΔE_s is very little influenced by the nonlocal corrections; for Fe $\Delta E_s = 25.0$ mRy/atom using LSD and $\Delta E_s = 23.7$ mRy/atom using GGA corrections (see Fig. 8).

The relative changes in the equilibrium atomic volumes ($\Delta V/V$) calculated using LSD and GGA functionals vary from 10 to 8% for the FM phases going from Fe to Co and Ni. $\Delta V/V$ decreases for the NM phases to about 7% but for a given material it does not depend on the type of structure. The softening of the bulk modulus is illustrated in Fig. 7. GGA corrects all the LSD error of B_0 for the stable crystal

TABLE V. Calculated equilibrium lattice constant (a_0), bulk modulus (B_0), magnetic moment (M_0), and cohesive energy (E_{coh}) for bcc FM Fe, hcp and fcc FM Co, and fcc FM Ni. USPP results for the LSD and GGA approximation are compared with previous calculations and experiment. The GGA results are in parentheses. For each calculation are also listed the abbreviations for the exchange-correlation type. For Fe the USPP ps1 reproduces the $4s^1 3d^7$ and ps2 the $3p^6 4s^1 3d^7$ atomic configurations.

Metal	Method	xc type LSD	(GGA)	a_0 (Å)		B_0 (Mbar)		M_0 (μ_B)		E_{coh} (eV)	
	LMTO [a]	CA-PZ	(PW91)	2.77	(2.85)	2.64	(1.82)	2.07	(2.29)		
	FLAPW [b]	VWN		2.76		2.66		2.08			
	FLAPW [c]	HL-vBH	(PW86)	2.76	(2.88)	2.51	(1.82)	2.19	(2.13)		
	FLAPW [d]		(PW91)		(2.84)		(1.86)		(2.17)		
	FLMTO [e]	VWN		2.77		2.52		2.02		7.73	
	LAPW [f]	HL-vBH	(PW91)	2.75	(2.83)	2.55	(1.72)	2.04	(2.17)		
bcc Fe	LCAO [g]	CA-PZ	(PW86)	2.78	(2.88)	2.64	(1.74)	2.08	(2.20)	7.32	(6.31)
	NCPP [h]	CA-PZ	(PW91)	2.76	(2.86)	2.26	(1.69)	2.01	(2.32)		
	This work (ps1)	CA-PZ	(PW91)	2.76	(2.86)	2.35	(1.55)	2.05	(2.32)	6.47	(5.15)
	This work (ps2)		(PW91)		(2.87)		(1.66)		(2.24)		(5.20)
	Exp [i]			2.87		1.68		2.22		4.28	
	LMTO [a]	CA-PZ	(PW91)	2.45	(2.52)	2.73	(2.24)	1.53	(1.61)		
hcp Co	This work	CA-PZ	(PW91)	2.45	(2.51)	2.42	(2.05)	1.52	(1.61)	6.88	5.62
	Exp [j]			2.51		1.91		1.72		4.39	
	LCAO [g]	CA-PZ	(PW86)	3.44	(3.56)	2.68	(2.14)	1.50	(1.63)	5.98	(4.52)
	NCPP [h]	CA-PZ	(PW91)	3.44	(3.54)	2.37	(2.04)	1.49	(1.66)		
	LMTO [a]	CA-PZ	(PW91)	3.44	(3.53)	2.70	(2.37)	1.52	(1.63)		
	LAPW [i]	HL-vBH		3.43		2.69		1.6			
fcc Co	This work	CA-PZ	(PW91)	3.45	(3.52)	2.42	(2.05)	1.52	(1.60)		
	Exp [j]			3.54							
	LMTO [a]	CA-PZ	(PW91)	3.44	(3.53)	2.46	(1.92)	0.60	(0.62)		
	FLAPW [d]		(PW91)		(3.52)		(2.00)		(0.60)		
	LCAO [g]	CA-PZ	(PW86)	3.42	(3.56)	2.50	(2.08)	0.59	(0.65)	5.45	(4.18)
	NCPP [h]	CA-PZ	(PW91)	3.44	(3.53)	2.39	(1.92)	0.60	(0.64)		
fcc Ni	This work	CA-PZ	(PW91)	3.43	(3.53)	2.55	(1.95)	0.59	(0.61)	6.09	(4.93)
	Exp [j]			3.52		1.86		0.61		4.44	

[a]Reference 24.
[b]Reference 62.
[c]Reference 59.
[d]Reference 76.
[e]Reference 66.
[f]Reference 70.
[g]Reference 77.
[h]Reference 27.
[i]Reference 72.
[j]Reference 78.

structure and modifies the elastic properties of some metastable phases in the fcc environment, because of the tendency of the GGA to stabilize magnetic ordering. For Co and Ni, LSD and GGA predict the correct ground state but GGA leads to a better agreement with experiment for the equilibrium properties.

The LSD cohesive energy E_{coh} for Fe, Co, and Ni is systematically overestimated by about 2.2, 2.5 and 1.6 eV/atom with respect to experiment. GGA corrections improve the prediction for all elements by reducing the LSD errors by about 1.3 to 1.1 eV/atom. The remaining discrepancy with experiment (of about 1.0 eV/atom for Fe to 0.5 eV/atom for Ni) may be overcome by improving the calculation of the total energy of the respective atoms (and its nonspherical multiplet states), through the use of orbital dependent potentials such as self-interactions corrections[45] (see also Sec. III A).

Table VI summarizes the LSD and GGA USPP calculations for different magnetic properties of bcc Fe, hcp Co, and fcc Ni. Nonlocal corrections emphasize the tendency towards spontaneous magnetizations, however the GGA effect on the spin magnetic moments is very small if compared to the associated magnetic energy corrections. The pressure dependence of the spin moment ($\partial \ln M_s / \partial P$) near the equilibrium for the ground state structure is nearly unaffected by GGA. This can also be seen from Fig. 9 where the LSD and GGA computed magnetic moments are plotted at different volumes for the FM phases of bcc, fcc, and hcp Fe, Co, and Ni. The magnetic moment for bcc Fe, hcp Co and fcc Ni is stable also at very high pressure. Consistent with previous

TABLE VI. Magnetic properties of bcc Fe, hcp Co, and fcc Ni using LSD and GGA USPP. The local-spin moment per atom M_s and the density of states (for up and down spin) $N(\epsilon_F)$ are computed at the experimental equilibrium lattice constant a_0. The pressure derivative $\partial \ln M_s/\partial P$ is calculated at the respective LSD and GGA theoretical equilibrium position. For FM bcc Fe two GGA USPP have been considered (USPP including $3p$ states in parenthesis).

	Units	Fe bcc			Co hcp			Ni fcc		
		LSD	GGA	exp	LSD	GGA	exp	LSD	GGA	exp
a_0	Å			2.866			2.507			3.524
M_s	μ_B/atom	2.23	2.33 (2.24)	2.22 [a]	1.58	1.62	1.72 [a]	0.60	0.62	0.61 [a]
$\partial \ln M_s/\partial \ln V$		0.85	0.86 (0.78)		0.50	0.45		0.51	0.50	
$\partial \ln M_s/\partial P$	1/ Mbar^{-1}	-0.36	-0.55 (-0.48)	-0.33 [b]	-0.20	-0.22	-0.22 [b]	-0.20	-0.26	-0.29 [b]
$N^{\uparrow}(\epsilon_F)$	states/eV atom	0.82	0.75 (0.85)		0.15	0.14		0.18	0.16	
$N^{\downarrow}(\epsilon_F)$	states/eV atom	0.25	0.27 (0.25)		0.74	0.74		1.70	1.65	

[a]Reference 78.
[b]Reference 58.

investigations[63] in Co the hcp and bcc structures maintain FM ordering at much higher pressure than does the fcc phase while in Ni the FM phase of the bcc structure becomes unstable at low pressure. The magnetic moments in Fe, Co, and Ni are reasonably well described with an USPP. For bcc Fe and the USPP without semicore states (ps1) GGA overestimates the spin moment ($M=2.33\mu_B$) and the exchange splitting of the uppermost $3d$ bands ($\xi_{\max}$) is 3.0 eV. The quality of the pseudopotential improves substantially when one describes the semicore electrons self consistently (ps2). The exchange splitting $\xi_{\max}$ in this case reduces from 3.0 eV to 2.8 eV and the spin moment reduces to $2.24\mu_B$. Moreover, if one considers the $PW91+$ approximation, including corrections of the gradient of the local-spin polarization ($\nabla\zeta$), M_0 reduces to $2.20\mu_B$.

For bcc, fcc, and hcp FM Co, at their equilibrium position the calculated LSD (GGA) spin moment are 1.65 (1.74), 1.55 (1.64), and 1.51 (1.61) μ_B per atom. For hcp Co the experimental moment is $1.72\mu_B$. This difference is explained by the estimated large orbital magnetic moment that is around $0.15\mu_B$/atom.[64] For fcc Ni, we found a LSD (GGA) spin local moment of 0.59 (0.61), while for bcc Ni a smaller magnetic moment of 0.43 (0.53) μ_B is obtained.

The GGA band structure is similar to the LSD one for all studied systems. A comparison of the eigenvalues calculated using both functional for few selected symmetry points for bcc Fe and fcc Ni is given in Table VII. For the exchange splitting the GGA brings only marginal corrections. The main effect is a general enhancement of the splitting of d states correlated with the increase of local moment and a reduction of the s-band splitting. For Fe the splitting of the s-like Γ_1 state is very small compared to the splitting of the d-like Γ'_{25} and Γ_{12} states and may become nearly zero or negative when GGA corrections are included. The nonsphericity of the potential influences the exchange splitting of the Γ_{12} and Γ'_{25} d states. In a muffin-tin approach they are expected to be quite similar while using the USPP we observe a large differences (0.49 eV with LSD), in good agreement with FLAPW calculations (0.52 eV). The enhancement of the Γ_{12} splitting and in particular with respect to the Γ'_{25} splitting by the GGA functional is also well reproduced.

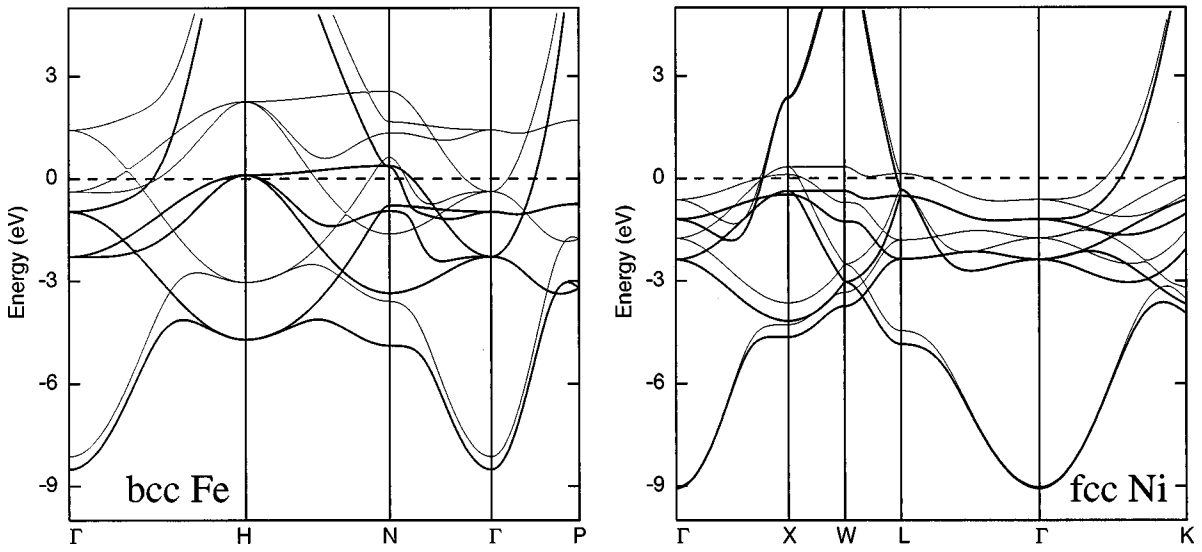

FIG. 6. Band structure for ferromagnetic bcc Fe and fcc Ni at the experimental lattice parameters. These bands have been calculated with the USPP and with the LSD approximation. The heavy curves are the majority spin bands while the light curves are for minority spin.

TABLE VII. Computed exchange splittings (ξ) and majority spin band energies ϵ (relative to the Fermi energy) at selected symmetry points for bcc Fe and fcc Ni at their experimental lattice parameter. USPP results are compared with all-electron values for both LSD and GGA functionals. The abbreviations for the exchange-correlation type are also listed. The abbreviation ps1 denotes the USPP for the $4s^1 3d^7$ atomic configuration while ps2 includes also $3p$ semicore states. The ps2 results are in parentheses.

	Iron				
	LCAO [a]	FLAPW		This work	
	(HL-vBH)	(HL-vBH)	(PW86)	(CA-PZ) ps1 (ps2)	(PW91) (ps2)
$\xi(\Gamma_1)$	0.17	0.42	-0.05	0.37 (0.37)	(0.18)
$\xi(\Gamma'_{25})$	1.82	1.90	1.69	1.96 (1.90)	(2.09)
$\xi(\Gamma_{12})$	2.18	2.42	2.57	2.45 (2.39)	(2.75)
$\xi(H_{12})$	1.51			1.72 (1.67)	(1.83)
$\xi(H_{25})$	2.11			2.21 (2.15)	(2.36)
$\xi(P_4)$	1.34	1.47	1.16	1.50 (1.45)	(1.50)
$\xi(P_3)$	2.10	2.49	2.65	2.52 (2.46)	(2.84)
$\xi(N_1)$	1.30			1.34 (1.30)	(1.35)
$\xi(N_2)$	1.65			1.78 (1.73)	(1.88)
$\epsilon(\Gamma_1)$	-8.12	-8.47	-8.25	-8.34 (-8.51)	(-8.34)
$\epsilon(\Gamma'_{25})$	-2.25	-2.27	-2.18	-2.26 (-2.28)	(-2.28)
$\epsilon(\Gamma_{12})$	-0.86	-0.96	-1.03	-0.97 (-0.97)	(-1.02)
$\epsilon(P_4)$	-3.17	-3.20	-3.07	-3.17 (-3.22)	(-3.17)
$\epsilon(P_3)$	-0.53	-0.75	-0.82	-0.75 (-0.75)	(-0.81)

	Nickel		
	LCAO [c]	This work	
	(vBH)	(CA-PZ)	(PW91)
$\xi(L_3)$	0.60	0.65	0.76
$\epsilon(L_3)$	-0.47	-0.51	-0.62
$\epsilon(X_5)$	-0.30	-0.37	-0.49

[a]Reference 61.
[b]Reference 59.
[c]Reference 60.

B. Structural properties

We will now investigate in more detail the accuracy of our USPP for predicting *structural* properties of Fe, Co, and Ni using both LSD and GGA functional. First, we compare our results to previous all-electron calculations. Second, we describe the GGA effects on different magnetic phases and as an application of the interplay between magnetism, pressure, and structure we illustrate the competitions between the NM, FM, and AF ordering at different volumes for the bcc, fcc, and hcp structures of Fe. Finally, we describe paths of tetragonal states of Fe, Co, and Ni between the magnetic fcc and bcc structure at a different pressure to test the accuracy of the USPP in describing the relative structural stability.

1. Comparison of USPP and AE results

The computed total energy difference with respect to the magnetic ground state, the equilibrium atomic volume, and the bulk modulus for the bcc, fcc, and hcp structures of Fe, Co, and Ni are compared to other calculations in Table VIII. This comparison demonstrates the accuracy of the USPP in predicting not only the equilibrium and bulk properties but also the structural energy differences between different magnetic configurations. Trends in structural magnetic energy differences are well reproduced, and the differences between USPP and AE methods are of the same magnitudes as the differences between full-potential linear muffin-tin orbitals (FLMTO) and FLAPW. For the fcc and hcp structures, their total energy differences (like in Co) are of the order of absolute accuracy of first-principle methods.

For the NM phases of Fe, Co and Ni the errors of USPP calculations with respect to full-potential calculations[62,65,66] are below ± 0.01 Å for the equilibrium lattice constant, in the ± 0.1 Mbar range for the bulk modulus and below 1 mRy/atom for the structural energy. Slightly larger differences are found for the structural energy differences between the magnetic bcc and fcc, and bcc and hcp structures. These errors are mainly related to the non self-consistent treatment of the core valence overlapping. Selected magnetic and structural energies for iron computed using LSD and GGA functional are given in Table IX and compared to other calculations.

For the studied systems a different choice of the spin-dependent correlation energy induces differences of 1 to 3

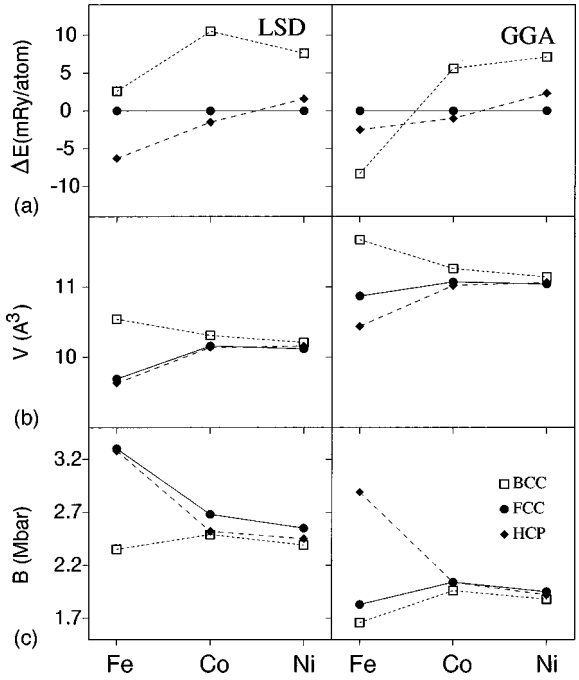

FIG. 7. Comparison between LSD and GGA for the structural properties of Fe, Co, and Ni. (a) hcp-fcc (filled diamonds) and bcc-fcc (squares) structural energy differences for the magnetic low-energy phases of Fe, Co, and Ni; (b) equilibrium volumes; and (c) bulk modulus of the magnetic low-energy phases of Fe, Co, and Ni for the bcc, hcp, and fcc structure.

mRy/atom in the magnetic energy using an USPP, similarly to the FLAPW results of Jansen and Peng,[67] and indirectly a decrease of the bulk modulus and changes in the local-spin moment. The largest effects of the spin parametrization concern the magnetic energy of bcc Fe (bcc Co) and the respective bcc-hcp and bcc-fcc structural energies difference.

Using GGA USPP calculations we have also studied the effect of including $3p$ states on the energetics of Fe. Without semicore states we found that the bcc FM phase is lower in

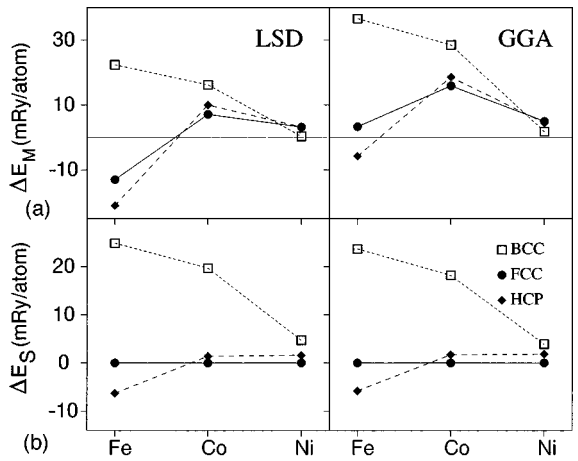

FIG. 8. Comparison between LSD and GGA for magnetic and paramagnetic total energy differences. (a) Differences in total energy between the FM and NM phases for the bcc, fcc, and hcp structure at their equilibrium lattice constant. (c) hcp-fcc (filled diamonds) and bcc-fcc (squares) structural energy differences between the NM phases of Fe, Co, and Ni.

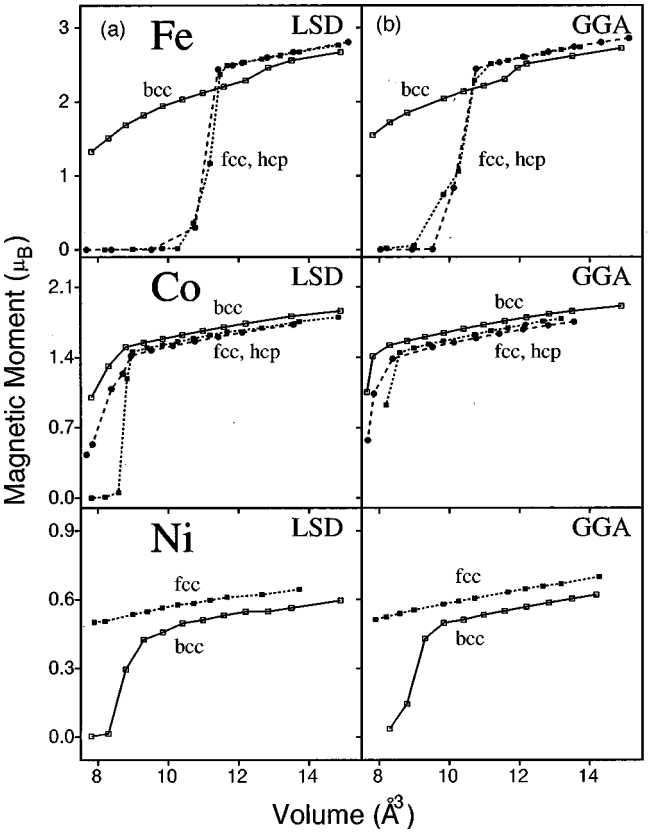

FIG. 9. Magnetic moment (M) for the ferromagnetic (FM) phases of bcc, hcp, and fcc Fe, Co, and Ni as a function of the volume V. Comparison between (a) LSD and (b) GGA USPP calculations.

energy than the fcc NM phase by 17.7 mRy, while treating the $3p$ electrons as valence states reduces the total energy difference to 12.9 mRy. This value agrees with an error of 1 mRy with the full-potential estimations of Abrikosov *et al.*[68] and of Singh *et al.*,[59] and is 2 mRy smaller than recent norm-conserving pseudopotential calculations of Cho and Scheffler[27] which use however the LAPW method to deal efficiently with the full core electron density but do not use semicore states.

The computed pressure-volume equations of state[69] for hcp Fe agree very well in the range of pressures from 0.2 to 3.0 Mbar with experiment by including semicore states effects. Without including the semicore states the theoretical pressure is about 7% smaller than the experimental value at a pressure larger than 1 Mbar. Under zero pressure the ground state of Fe is bcc FM and the hcp structure becomes stable above a critical pressure of 170 kbar, which is in the range of the measured pressures of 130–150 kbar[69] and is in a nonmagnetic state. The GGA relaxed c/a ratio for the NM hcp structure is of 1.58 consistent with previous LDA results.[66,65]

2. Magnetic phases of Fe and Co

To give an example of competition between different magnetic structures we show in Fig. 10 the total energies and local magnetic moments of FM, AF, and NM states of bcc, fcc, and hcp Fe versus atomic volume. These results have been obtained using the USPP which includes the semicore states and the GGA approximation. Neglecting the self-

TABLE VIII. Structural properties of Fe, Co, and Ni. Comparison between USPP and others calculations using the LSD approximation. The structural energies ($E-E_{\mathrm{FM}}$), the equilibrium atomic volume (V_0), and the bulk modulus (B_0) are expressed in mRy/atom , Å^3, and Mbar units, respectively.

		Iron			
Method (xc type)		FM bcc	NM bcc	NM fcc	NM hcp
This work	$E-E^{\mathrm{FM}}_{\mathrm{bcc}}$	0.0	22.4	-2.6	-8.9
(ps1)	V_0	10.54	9.89	9.69	9.63
(CA-PZ)	B_0	2.35	3.08	3.31	3.28
FLAPW [a]	$E-E^{\mathrm{FM}}_{\mathrm{bcc}}$	0.0	21.0	-4.0	
(VWN)	V_0	10.48	9.83	9.62	
	B_0	2.66	3.14	3.44	
FLMTO [b]	$E-E^{\mathrm{FM}}_{\mathrm{bcc}}$	0.0	19.5	-5.9	-7.9
(VWN)	V_0	10.60	9.95		9.65
	B_0	2.52	3.20		
		Cobalt			
Method (xc type)		FM bcc	FM fcc	FM hcp	
This work	$E-E^{\mathrm{FM}}_{\mathrm{hcp}}$	12.0	1.5	0.0	
(CA-PZ)	V_0	10.31	10.17	10.14	
	B_0	2.49	2.54	2.52	
LAPW [c]	$\mathrm{E\text{-}E}^{\mathrm{FM}}_{\mathrm{hcp}}$	10.9	2.0	0.0	
(HL-vBH)	V_0	10.28	10.09		
	B_0	2.54	2.69		
LMTO [d]	$E-E^{\mathrm{FM}}_{\mathrm{hcp}}$	8.2	2.2	0.0	
(CA-PZ)	V_0	10.39	10.20	10.20	
	B_0	2.71	2.98	2.74	
		Nickel			
Method (xc type)		FM bcc	FM fcc	FM hcp	
This work	$E-E^{FM}_{\mathrm{fcc}}$	7.6	0.0	1.6	
(CA-PZ)	V_0	10.21	10.12	10.16	
	B_0	2.39	2.56	2.45	
FLMTO [b]	$E-E^{\mathrm{FM}}_{\mathrm{fcc}}$	5.9	0.0		
LMTO [d]	$E-E^{\mathrm{FM}}_{\mathrm{fcc}}$	2.8	0.0		
(CA-PZ)	V_0	10.18	10.21		
	B_0	2.65	2.71		

[a]Reference 62.
[b]Reference 66.
[c]Reference 72.
[d]Reference 24.

TABLE IX. Energetics of Fe. Comparison between USPP and others calculations with LSD and GGA approximation. ΔE_s is the total energy difference of NM bcc and NM fcc phases, ΔE_s^m is the total energy difference of FM bcc and NM fcc phases and ΔE^m is the total energy difference between the NM and FM phases of the bcc crystal structure. All energies are in mRy/atom unit.

Metal	Method	xc type		ΔE_s		ΔE_s^m		ΔE^m	
		LSD	(GGA)						
	LMTO [a]	CA-PZ	(PW91)	22.0	(20.8)	4.5	(-10.4)	17.5	(31.2)
	FPLMTO [b]	VWN				5.9		19.5	
Fe	FLAPW [c]	HL-vBH	(PW86)	25.8	(21.2)	4.1	(-13.9)	21.7	(35.1)
	FLAPW [d]	VWN		27.0		6.0		21.0	
	NCPP [e]	CA-PZ	(PW91)	24.6	(23.1)	4.4	(-14.9)	20.2	(38.0)
	This work (ps1)	CA-PZ	(PW91)	25.0	(22.9)	2.6	(-17.7)	22.4	(40.6)
	This work (ps2)	CA-PZ	(PW91)		(23.7)		(-12.9)		(36.6)

[a]Reference 24.
[b]Reference 66.
[c]Reference 59.
[d]Reference 62.
[e]Reference 27.

consistent description of semicore states we obtain the same magnetic phase diagram and volume dependence, however the magnetic energies of the AF and FM phases are enhanced by about 1 and 3 mRy/atom, respectively. As examples of the most usual AF states, the AF1 and AF2 antiferromagnetic configurations [which can be described as superlattices of period $p=1$ and layer orientation $G=(001)$ and $G=(111)$, respectively] are computed. The total energies have been computed without constraining the magnetic moments and low-spin ferromagnetic configurations for fcc Fe are not shown in Fig. 10. The studied magnetic phases are more stable than the respective NM phases. The relative hierarchy between the FM, AF1 and AF2 magnetic configurations depends on the volume and the basic crystal structure. Their total energy differences change considerably along tetragonal paths. GGA corrections enhance the magnetic energies of the studied magnetic configurations but do not affect the critical volume range in fcc Fe where the AF-FM transition occurs. The fcc-hcp crossover is possible as shown in Fig. 10 by increasing the volume. At a small volume, hcp Fe is more stable than NM fcc Fe of about 5.8 (6.3) mRy/atom using a GGA (LDA) approximation. At expanded volume, FM hcp Fe lies however higher in energy than FM fcc Fe, indicating the instability of the hcp lattice (over fcc) at high temperature and under normal pressure condition.

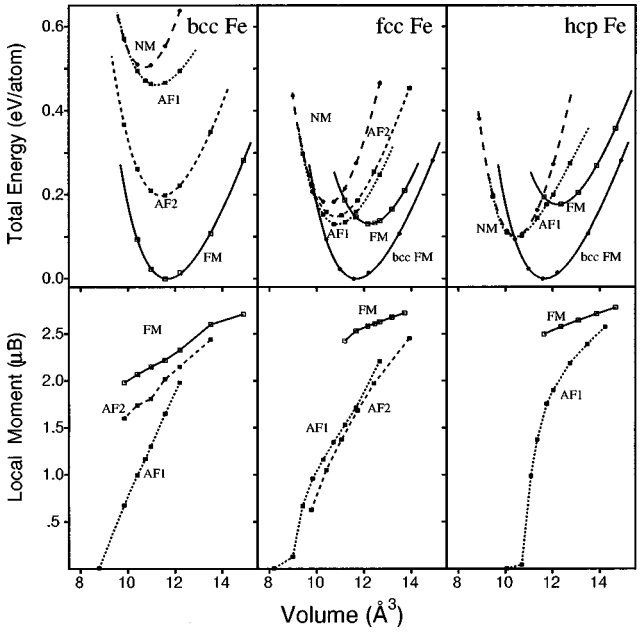

FIG. 10. Total energy per atom for nonmagnetic NM, antiferromagnetic (AF1,AF2) and ferromagnetic (FM) phases of bcc, fcc, and hcp Fe as a function of the volume relative to the FM bcc ground state energy. These total energy results refer to the USPP calculations including $3p$ states and with GGA approximation.

Our USPP calculations predict correctly the FM hcp structure as ground state for Co using both LSD and GGA functionals. Unlike Cr, Mn, and Fe which have stable AF states in the fcc structure, the FM state is the most stable in all studied structure of Co. FM hcp Co is however only 1.5 mRy/atom lower in energy with respect to FM fcc Co which is less stable than hcp and bcc crystal structure at high pressure. The hcp-fcc structural stability depends on the magnetic state. In fact, our nonmagnetic calculations of fcc and hcp Co predict a lower energy for the fcc structure with an hcp-fcc energy barrier of about 2 mRy/atom. The stabilization of hcp Co by magnetic ordering that we recover using both LSD and GGA functionals is consistent with previous LMTO LSD results of Min, Oguchi, and Freeman[63] and also with more recent GGA FPLMTO calculations of Abrikosov *et al.*[68] which explain these anomalous structural competitions in terms of a canonical spin-down d-bands analysis. The exact mechanism of the hcp-fcc structural transformations however is still an open problem. Moreover, in analogy with the case of bcc Fe, the relative stability of FM bcc Co over the NM fcc and hcp structure is increased when using GGA. This effect may be of importance for a correct description of the bcc → hcp structural transformation properties for the Fe-Co alloy.

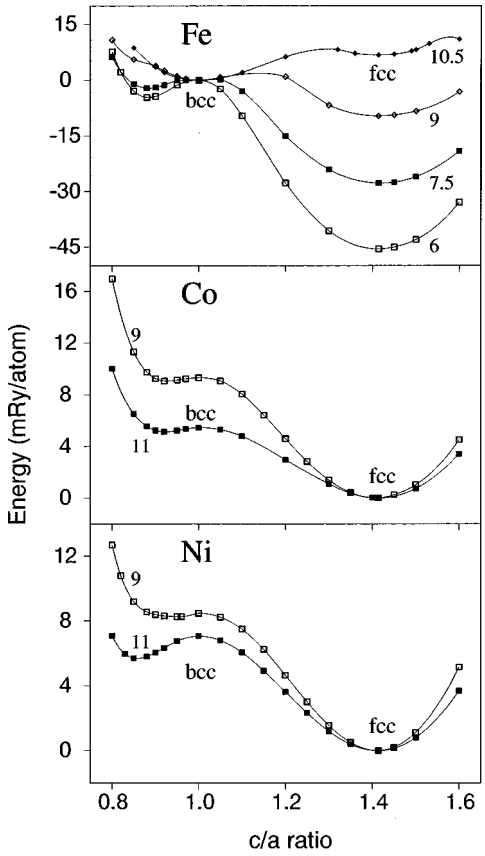

FIG. 11. Total energy change along the tetragonal distortions of the Bain path of bct Fe, Co, and Ni at different atomic volumes (in $Å^3$). These energy are obtained using USPP and the GGA approximation.

3. Tetragonal states of Fe, Co, and Ni

As a final application we have tested our USPP for computing tetragonal states at various volumes. For describing the elastic properties along the tetragonal path, the total energy of the body-centered tetragonal structure (bct) for the FM phases of Fe has been computed for a different c/a ratio along the Bain path. The bcc structure corresponds to $c/a=1$; the fcc structure to $c/a=\sqrt{2}$. The GGA USPP total energies of bct Fe illustrated in Fig. 11 at different volumes ($V=ca^2/2$) compare well with the GGA LAPW results displayed in Fig. 3(b) of Ref. 70. Both bcc and fcc structure are found to be elastically stable under normal pressure condition. Along this path, at high pressure ($V<8$ $Å^3$) the bcc crystal structure is elastically unstable with respect to a tetragonal strain towards the global minimum in the fcc structure or towards the local minima of a tetragonal unit cell with $c/a=0.88$. The Fe magnetic moment for bct Fe is not constant along the Bain path and depends sensibly on the pressure and c/a ratio. At high pressure and for $c/a<1.3$ the moment is still large affecting the respective $P\Delta V$ term of the fcc-bcc Gibbs energy difference.[71]

Differently to Fe, along the tetragonal path for both Co and Ni the stable cubic structure is fcc ($c/a=\sqrt{2}$) with $a_{\mathrm{fcc}}=2.5$ Å; the bcc crystal structure correspond to the saddle point (with $a=2.82$ Åfor Co and $a=2.81$ Åfor Ni) and a metastable tetragonal structure is found at $c/a=0.92$ for Co and $c/a=0.95$ for Ni at constant $V=11$ $Å^3$. The elastic properties of bct Co versus c/a ratio are in good agreement with previous LSD LAPW investigations of Liu and Singh.[72] Using GGA, we found only a slightly smaller bcc-fcc energy barrier of 5.6 mRy.

Finally, all these results indicate that our USPP allow for an accurate description (as full-potential methods) of elastic instability and structural energies between different magnetic configurations and different structure. We believe that these USPP may be used in the future for testing the spin dependence of new exchange-correlation potentials, and in combination with finite temperature models may also be used to quantify the importance of different type of thermal magnetic excitations for fcc Fe and Co at high temperature.[73]

VII. CONCLUSION

In this paper, we have shown that spin polarized calculations employing ultrasoft pseudopotentials can be used efficiently to study the magnetic and structural behavior of magnetic systems with an accuracy comparable to the best all-electron methods. More specifically, we have shown that the USPP approach is able to accurately reproduce all-electron results within both the LSD and GGA schemes and we have also shown that nonlinear core corrections in the treatment of the exchange-correlation energy are necessary for describing correctly the magnetic properties. These ultrasoft pseudopotentials use very modest energy cutoffs, if compared to standard soft normconserving pseudopotentials and are designed for very accurate spin-polarized *ab initio* electronic structure calculations.

We have applied these USPP to study the equilibrium properties and the magnetic behavior of Fe, Co, and Ni in different environments, ranging from the free atoms over dimers and monolayers to the solid phases. We have found that, except for the atoms, in all other studied systems the GGA functional (in the PW91 form) is able to correct most of the LSD errors. Moreover, the transferability of these pseudopotentials has also been tested by studying the structural instability at high pressure and to compute the energy differences between various magnetic structures. For Fe, the usage of the GGA functional and inclusion of the $3p$ semicore states has led to the best overall pseudopotential for high-pressure applications and to accurate magnetization energies.

The accuracy of these USPP is comparable to full-potential all-electron methods and at the level of being able to discuss phase stability on a 1 mRy/atom scale. They may be used very efficiently in combination with *ab initio* molecular dynamic programs, with fixed-spin-moment schemes[73] or with cluster expansion techniques[74] for the study of electronic structure, relaxation properties, surface magnetism, and magnetism in amorphous systems.

ACKNOWLEDGMENTS

This work has been supported by the Austrian Science Fund under Project No. P11353-PHYS. One of us (E.G.M) acknowledges support by the Swiss National Science Foundation under Grant No. 8220-042840. We thank G.A. de Wijs for a critical reading of the manuscript.

[1] R. Car and M. Parrinello, Phys. Rev. Lett. **55**, 2471 (1985).
[2] M. C. Payne, M. P. Teter, D. C. Allan, T. A. Arias, and J. D. Joannopoulos, Rev. Mod. Phys. **64**, 1045 (1992); M. P. Teter, M. C. Payne, and D. C. Allan, Phys. Rev. B **40**, 12 255 (1989).
[3] G. Kresse and J. Furthmüller, Comput. Mater. Sci. **6**, 15 (1996); Phys. Rev. B **55**, 11 196 (1996).
[4] A. Pasquarello, K. Laasonen, R. Car, C. Lee, and D. Vanderbilt, Phys. Rev. Lett. **69**, 1982 (1992).
[5] G. Kresse and J. Hafner, Phys. Rev. B **47**, 558 (1993).
[6] P. E. Blöchl, Phys. Rev. B **50**, 17 953 (1994).
[7] D. M. Bylander and L. Kleinman, Phys. Rev. B **46**, 9837 (1992).
[8] G. Kresse and J. Hafner, J. Phys. Condens. Matter **6**, 8245 (1994).
[9] D. R. Hamman, M. Schlüter, and C. Chiang, Phys. Rev. Lett. **43**, 1494 (1979); G. B. Bachelet, D. R. Hamann, and M. Schlüter, Phys. Rev. B **26**, 4199 (1982); D. R. Hamann, *ibid.* **40**, 2980 (1989).
[10] G. P. Kerker, J. Phys. C **13**, L189 (1980); D. Vanderbilt, Phys. Rev. B **32**, 8412 (1985); E. L. Shirley *et al.*, *ibid.* **40**, 3652 (1989); N. Troullier and J. L. Martins, *ibid.* **43**, 1993 (1991); J. S. Lin *et al.*, *ibid.* **47**, 4174 (1993).
[11] A. M. Rappe, K. M. Rabe, E. Kaxiras, and J. D. Joannopoulos, Phys. Rev. B **41**, 1227 (1990).
[12] D. Vanderbilt, Phys. Rev. B **41**, 7892 (1990).
[13] K. Laasonen, A. Pasquarello, R. Car, C. Lee, and D. Vanderbilt, Phys. Rev. B **47**, 10 142 (1993).
[14] A. Eichler, K. P. Bohnen, H. Reichhardt, and J. Hafner, Phys. Rev. B (to be published).
[15] A. Eichler, G. Kresse, and J. Hafner, Phys. Rev. Lett. **77**, 1119 (1996); A. Eichler *et al.*, Surf. Sci. **346**, 300 (1995).
[16] G. Kresse and J. Hafner, Phys. Rev. B **55**, 7539 (1997).
[17] W. Kohn and L. J. Sham, Phys. Rev. **140**, A1 133 (1965).
[18] R. M. Dreizler and E. K. U. Gross, *Density Functional Theory* (Springer Verlag, Berlin, 1990); R. G. Parr and W. Yang, *Density Functional Theory of Atoms and Molecules* (Oxford, New York, 1989).
[19] O. Gunnarsson, B. I. Lundqvist, and J. W. Wilkins, Phys. Rev. B **10**, 1319 (1974); O. Gunnarsson and B. I. Lundqvist, *ibid.* **14**, 4272 (1975); O. Gunnarsson, J. Phys. F **6**, 587 (1976).
[20] D. C. Langreth and M. J. Mehl, Phys. Rev. B **28**, 1809 (1983); J. P. Perdew, *ibid.* **33**, 8882 (1986); A. D. Becke, Phys. Rev. A **38**, 3098 (1988).
[21] J. P. Perdew, in *Electron Structure of Solids '91*, edited by P. Ziesche and H. Eschrig (Akademie Verlag, Berlin, 1991), p. 11; J. P. Perdew and Y. Wang, Phys. Rev. B **45**, 13 244 (1992); and references therein.
[22] J. P. Perdew, K. Burke, and M. Ernzerhof, Phys. Rev. Lett. **77**, 3865 (1996); J. P. Perdew, K. Burke, and Y. Wang, Phys. Rev. B **54**, 16 533 (1996).
[23] P. Bagno, O. Jepsen, and O. Gunnarsson, Phys. Rev. B **40**, 1997 (1989).
[24] B. Barbiellini, E. G. Moroni, and T. Jarlborg, J. Phys. Condens. Matter **2**, 7597 (1990); E. G. Moroni (unpublished).
[25] S. G. Louie, S. Froyen, and M. L. Cohen, Phys. Rev. B **26**, 1738 (1982).
[26] H. S. Greenside and M. A. Schlüter, Phys. Rev. B **27**, 3111 (1983).
[27] J. Cho and M. Scheffler, Phys. Rev. B **53**, 10 685 (1996).
[28] Jing Zhu, X. W. Wang, and S. G. Louie, Phys. Rev. B **45**, 8887 (1992).
[29] P. Ballone and R. O. Jones, Chem. Phys. Lett. **233**, 632 (1995); J. Cho and M. Kang, Phys. Rev. B **52**, 9159 (1995).
[30] X. Gonze, P. Käckell, and M. Scheffler, Phys. Rev. B **41**, 12 264 (1990); X. Gonze, R. Stumpf, and M. Scheffler, *ibid.* **44**, 8503 (1991); A. Klein, *ibid.* **51**, 16 608 (1995).
[31] L. Vočadlo, G. A. de Wijs, G. Kresse, M. J. Gillan, and G. D. Price (unpublished).
[32] D. M. Wood and A. Zunger, J. Phys. A **18**, 1343 (1985).
[33] P. Pulay, Chem. Phys. Lett. **73**, 393 (1980); C. G. Broyden, Math. Comput. **19**, 577 (1965); D. D. Johnson, Phys. Rev. B **38**, 12 087 (1988).
[34] D. M. Ceperly and B. J. Alder, Phys. Rev. Lett. **45**, 566 (1980).
[35] J. Perdew and A. Zunger, Phys. Rev. B **23**, 5048 (1981).
[36] J. A. White and D. M. Bird, Phys. Rev. B **50**, 4954 (1994).
[37] U. von Barth and L. Hedin, J. Phys. C **5**, 1629 (1972).
[38] S. H. Vosko, L. Wilk, and M. Nusair, Can. J. Phys. **58**, 1200 (1980).
[39] G. Ortiz and P. Ballone, Phys. Rev. B **50**, 1391 (1994).
[40] H. J. Monkhorst and J. D. Pack, Phys. Rev. B **13**, 5188 (1976).
[41] P. E. Blöchl, O. Jepsen, and O. K. Andersen, Phys. Rev. B **49**, 16 223 (1994).
[42] A. De Vita and M. J. Gillan, J. Phys. Condens. Matter **3**, 6625 (1991); A. De Vita, Ph.D. thesis, Keele University, 1992.
[43] M. Methfessel and A. T. Paxton, Phys. Rev. B **40**, 3616 (1989).
[44] J. Harris and R. O. Jones, J. Chem. Phys. **70**, 830 (1979).
[45] S. Baroni, J. Chem. Phys. **80**, 5703 (1984).
[46] B. H. Botch, T. H. Dunning, Jr., and J. F. Harrison, J. Chem. Phys. **75**, 3466 (1981); C. H. Bauschlicher, Jr., S. P. Walch, and H. Partridge, *ibid.* **76**, 1033 (1982).
[47] H. M. Hulburt and J. O. Hirschfelder, J. Chem. Phys. **9**, 61 (1941).
[48] P. A. Montano and G. K. Shenoy, Solid State Commun. **35**, 53 (1980); H. Purdum *et al.*, Phys. Rev. B **25**, 4412 (1982); L. Lian, C. X. Su, and P. B. Armentrout, J. Chem. Phys. **72**, 4072 (1992); M. Moskovits, D. P. DiLella, and W. Limm, *ibid.* **80**, 626 (1984).
[49] S. Dhar and N. R. Kestner, Phys. Rev. B **38**, 1111 (1988); J. L. Chen, C. S. Wang, K. A. Jackson, and M. R. Pederson, *ibid.* **44**, 6558 (1991).
[50] M. Castro and D. R. Salahub, Phys. Rev. B **49**, 11 842 (1994).
[51] T. Noro, C. Ballard, M. H. Palmer, and H. Tatewaki, J. Chem. Phys. **100**, 452 (1994).
[52] L. Mitas, Phys. Rev. A **49**, 4411 (1994); Comput. Phys. Commun. **96**, 107 (1996).
[53] M. Weinert and S. Blügel, in *Magnetic Multilayers*, edited by L.H. Bennet and R.E. Watson (World Scientific, Singapore, 1993).
[54] R. Pentcheva, Diplomarbeit in Physics, Uni Köln, 1996; S. Blügel, *Ground-state Properties of Ultrathin Magnetic Films Habilitations-schrift* (RWTH, Aachen, 1995).
[55] E.G. Moroni and J. Hafner (unpublished).
[56] F. D. Murnaghan, Proc. Natl. Acad. Sci. USA **30**, 244 (1944); F. Birch, J. Geophys. Res. **57**, 227 (1952).
[57] V. L. Moruzzi, J. F. Janak, and A. R. Williams, in *Calculated Electronic Properties of Metals* , (Pergamon, New York, 1978).
[58] E. I. Kondorskii and V. L. Sedov, Sov. Phys. JETP **11**, 561 (1960); J. S. Kouvel and C. C. Hartelius, J. Appl. Phys. **35**, 940 (1964).
[59] D. J. Singh, W. E. Pickett, and H. Krakauer, Phys. Rev. B **43**, 11 628 (1991).
[60] C. S. Wang and J. Callaway, Phys. Rev. B **15**, 298 (1977).
[61] J. Callaway and C. S. Wang, Phys. Rev. B **16**, 2095 (1977).
[62] C. S. Wang, B. M. Klein, and H. Krakauer, Phys. Rev. Lett. **54**,

1852 (1985); K. B. Hathaway, H. J. F. Jansen, and A. J. Freeman, Phys. Rev. B **31**, 7603 (1985).
[63] B. J. Min, T. Oguchi, and A. J. Freeman, Phys. Rev. B **33**, 7852 (1986); V. L. Moruzzi, Phys. Rev. Lett. **57**, 2211 (1986).
[64] B. Szpunar and P. Strange, J. Phys. F **15**, L165 (1985); G. H. O. Daalderop, P. J. Kelly, and M. F. H. Schuurmans, Phys. Rev. B **41**, 11 919 (1990).
[65] A. T. Paxton, M. Methfessel, and H. M. Polatoglou, Phys. Rev. B **41**, 8127 (1990).
[66] T. Kraft, M. Methfessel, M. van Schilfaarde, and M. Scheffler, Phys. Rev. B **47**, 9862 (1993); T. Kraft, Dissertation, Berlin Technological University.
[67] H. J. F. Jansen and S. S. Peng, Phys. Rev. B **37**, 2689 (1988); J. M. MacLaren, D. P. Clougherty, and R. C. Albers, *ibid.* **42**, 3205 (1990).
[68] I. A. Abrikosov *et al.*, Phys. Rev. B **54**, 3380 (1996).
[69] H. K. Mao, Y. Wu, L. Chen, J. F. Shu, and A. P. Jephcoat, J. Geophys. Res. **95**, 21 737 (1990); A. P. Jephcoat, H. K. Mao, and P. M. Bell, *ibid.* **91**, 4677 (1986).
[70] L. Stixrude, R. E. Cohen, and D. J. Sing, Phys. Rev. B **50**, 6442 (1994); L. Stixrudel and R. E. Cohen, Geophys. Res. Lett. **22**, 125 (1995).
[71] E. G. Moroni and T. Jarlborg, Europhys. Lett. **33**, 223 (1996).
[72] A. Y. Liu and D. J. Singh, Phys. Rev. B **47**, 8515 (1993); D. J. Singh, *ibid.* **45**, 2260 (1992).
[73] M. Uhl, L. M. Sandratskii, and J. Kübler, Phys. Rev. B **50**, 291 (1994); M. Uhl and J. Kübler, Phys. Rev. Lett. **77**, 334 (1996).
[74] S. Wei and A. Zunger, Phys. Rev. B **48**, 6111 (1993); V. Ozolins, Ph.D. dissertation, Royal Institute of Technology, 1996.
[75] M. D. Morse *et al.*, J. Chem. Phys. **80**, 5400 (1984).
[76] H. C. Herper, E. Hoffmann, and P. Entel, J. Phys. IV, C (1997) (to be published).
[77] T. C. Leung, C. T. Chan, and B. N. Harmon, Phys. Rev. B **44**, 2923 (1991).
[78] C. Kittel, *Introduction to Solid State Physics*, 6th ed. (Wiley, New York, 1986).